Article:
Delor, M, Archer, S.A., Keane, T. orcid.org/0000-0003-4975-0868 et al. (5 more authors) (2017) Directing the path of light-induced electron transfer at a molecular fork using vibrational excitation. Nature Chemistry, 9 (11). pp. 1099-1104. ISSN 1755-4330

https://doi.org/10.1038/nchem.2793

Directing the path of light-induced electron transfer at a molecular fork using vibrational excitation

Milan Delor,[1#] Stuart A. Archer,[1] Theo Keane,[1] Anthony J.H.M. Meijer,[1] Igor V. Sazanovich,[2] Gregory M. Greetham,[2] Michael Towrie,[2] and Julia A. Weinstein[1*]*

1. Department of Chemistry, University of Sheffield, Sheffield S3 7HF, U.K.

2. Central Laser Facility, Research Complex at Harwell, Rutherford Appleton Laboratory, Chilton, Oxfordshire, OX11 0QX, U.K.

#. Current address: Department of Chemistry, University of California, Berkeley, CA94720, USA.

Abstract

Ultrafast electron transfer in condensed-phase molecular systems is often strongly coupled to intramolecular vibrations that can promote, suppress and direct electronic processes. Recent experiments exploring this phenomenon proved that light-induced electron transfer can be strongly modulated by vibrational excitation, suggesting a new avenue for active control over molecular function. Here, we achieve the first example of such explicit vibrational control through judicious design of a Pt(II)-acetylide charge-transfer Donor-Bridge-Acceptor-Bridge-Donor "fork" system: asymmetric ^{13}C isotopic labelling of one of the two -C≡C-bridges makes the two parallel and otherwise identical Donor→Acceptor electron-transfer pathways structurally distinct, enabling independent vibrational perturbation of either. Applying an ultrafast UV_{pump}(excitation)-IR_{pump}(perturbation)-IR_{probe}(monitoring) pulse sequence, we show that the pathway that is vibrationally perturbed during UV-induced electron-transfer is dramatically slowed down compared to its unperturbed counterpart. One can thus choose the dominant electron transfer pathway. The findings deliver a new opportunity for precise perturbative control of electronic energy propagation in molecular devices.

Main Text

Controlling the function of future advanced materials demands a profound understanding of energy-matter interactions in molecular systems at the quantum level.[1] There is a growing consensus that energy- and electron-transfer processes occurring far away from equilibrium in condensed-phase systems on femto-to-picosecond timescales do not conform to the Born-Oppenheimer approximation. Indeed, nuclear and electronic wave functions often strongly interact with each other, leading to exotic phenomena whereby vibrational motion can mediate and dictate the rate and efficiency of electronic transitions.[2–5] With overwhelming evidence that nuclear-electronic (vibronic) interactions play a crucial role in a broad range of systems, including light harvesting and conversion in photosynthetic organisms,[6–11] this phenomenon represents a tremendous opportunity to acquire deeper knowledge and control over the structural traits that govern molecular function and reactivity.

Recent efforts led by Rubtsov *et al.*,[12,13] Bakulin *et al.*,[14] and our group[15,16] have shown that one way to experimentally exploit vibronic coupling to modulate molecular function is to introduce targeted vibrational excitation along specific reaction co-ordinates using ultrafast mid-infrared (IR) pulses. This approach enables promoting or suppressing electronic transitions, notably photo-induced electron transfer (ET), an elementary process that pervades the natural world. Although the demonstrated excited state modulations have been remarkably efficient, up to 100% suppression in one case,[15] predictive and directive control of electron transfer in the condensed phase has not been achieved yet.

To realise precise and targeted vibrational control over light-induced molecular function based on these emerging experimental approaches, and on pioneering theoretical studies on vibrational control in molecular interferometers by Beratan, Skourtis and co-workers,[17–20] we designed a "fork" Donor─Bridge─Acceptor─Bridge─Donor molecule with two parallel, electronically identical but structurally identifiable electron transfer pathways. This key requirement has been fulfilled by using acetylide-bridged assembly with selective ^{13}C-isotopic substitution of one of the two C≡C bridges that connect two identical electron donors D to a single acceptor A, D─(^{13}C≡^{13}C)─A─(^{12}C≡^{12}C)─D (Figure 1). Such non-intrusive modification makes the two electronically identical D→B→A pathways of ET vibrationally distinct, permitting selective excitation of either by mid-infrared light without modifying electronic behaviour.

Using this new molecular platform, a UV_{pump}-IR_{pump}-IR_{probe} pulse sequence can be employed to direct electron transfer: the UV_{pump} populates a gateway charge transfer state from which either of the charge separated states $D^{+\bullet}$─B─$A^{-\bullet}$, herein designated as *^{13}CSS* or *^{12}CSS* depending on their location on the ^{13}C─ or ^{12}C─arm, respectively, are formed at equal rates (Supplementary Fig. 3); the narrow-band IR_{pump} then selectively excites bridging vibrational modes associated with one of the two competing ET pathways in the course of ET; and finally, the IR_{probe} is used to spectrally monitor the changes in the population of the CSSs caused by the IR_{pump}. Vibrational excitation asymmetrically perturbs the ET probabilities at the excited state "crossroad" experienced by the system. Any difference in the yield of either CSS caused by IR excitation can be quantified by tuning the IR_{pump} pulse to a specific frequency and recording transient IR spectra with and without this intermediate vibrational excitation. Using this approach we demonstrate, for the first time, active control over the spatial direction of intramolecular electron transfer with mid-infrared light.

Results and Discussion

The chosen model compound that bears two parallel and electronically identical pathways is $[(CO_2Et)_2bpy]Pt[C{\equiv}C\text{-}p\text{-}C_6H_4CH_2(PTZ)]_2$ **(1)**, a well-studied charge-transfer system that possesses one acceptor group, 4,4'-$(CO_2Et)_2$-2,2'-bpy ($(CO_2Et)_2bpy$), and two phenothiazine donor groups (PTZ) connected via IR-active ─C≡C─ bridges to a Pt centre, Figure 1b.[21] The excited-state dynamics of **1** in solution (Figure 1d) have been previously resolved by ultrafast transient absorption,[21] time-resolved infrared[22] and photoinduced transient displacement current[23] measurements: excitation with 400 nm light populates a {Pt/C≡C→bpy} Metal-to-Ligand-Charge-Transfer state that is assumed to rapidly undergo intersystem crossing to the triplet manifold.[21,23] In polar solvents, subsequent electron transfer from the PTZ-donor to the oxidised Pt/CC moiety populates a final charge-separated state, CSS, where either of the two identical PTZ groups is oxidised.

Vibrationally decoupling the two electron transfer pathways

The key modification made to **1** to realise IR-control is the aforementioned isotopic labelling of one of the acetylide bridging groups as ^{13}C≡^{13}C (the new molecule, ^{13}C≡^{13}C/^{12}C≡^{12}C, is hereafter referred to as **1***), which makes the two donor arms of the molecule spectroscopically distinct in the mid-IR region.[24] We confirmed that the excited state behaviour of **1*** is not affected by isotopic labelling, and is identical to that of the symmetric fully labelled **^{13}1**, and of the unlabelled **1** (see Supplementary Fig. 1-3 for transient absorption data, Supplementary Fig. 5 for TRIR data).

The FTIR spectrum of **1*** is shown in Figure 2. According to a reduced mass analysis, one expects two distinct acetylide stretching vibrations separated by approximately 80 cm^{-1} in **1***; however, we observe three bands, one ^{12}C≡^{12}C localized stretch at 2123 cm^{-1} ($\nu(^{12}C)$) and a doublet around 2040

cm^{-1}, where $\nu(^{13}C)$ is anticipated. Analysis of the calculated fully-anharmonically corrected vibrations of the molecule shows that the observed doublet is due to a combination band of two vibrations localized on the ^{13}C-arm of the molecule in resonance with the $\nu(^{13}C)$ fundamental, leading to quantum mechanical mixing and intensity borrowing between the two modes.[24,25]

A prerequisite to ensure that mode-selective excitation with an IR_{pump} leads to localised excitations on either arm of the molecule is that $\nu(^{13}C)$ and $\nu(^{12}C)$ are decoupled. To ascertain that this condition is fulfilled, two-dimensional IR experiments (2DIR), which can be used to probe off-diagonal coupling elements between sets of vibrations,[26] were performed on this system. Figure 2b displays the 2DIR spectrum in the ground electronic state of **1*** at an IR_{pump}-IR_{probe} delay of 3 ps. Negative-positive peak pairs along the diagonal correspond to de-population of the ground state and associated population of the v=1 state, giving rise to ground state bleaching, stimulated emission (v=1→0), and excited state absorption (v=1→2) red-shifted from the ground state bleach by the vibrational anharmonicity (typically ~ 20 cm^{-1} for C≡C stretches in Pt-acetylides[16]). Coupling between the $\nu(^{12}C)$ and $\nu(^{13}C)$ vibrations would appear as off-diagonal (cross-) peaks. Any cross-peaks present in the spectra at 3 ps (and up to 50 ps) are negligible, indicating that, crucially, isotopic substitution successfully decouples $\nu(^{12}C)$ and $\nu(^{13}C)$. The large difference in intensities between the two diagonal peaks are primarily due to faster decay of the ^{13}C-stretch vibration ($\tau = 2.5 \pm 0.4$ ps) than of the ^{12}C-stretch ($\tau = 5.6 \pm 0.2$ ps) (Figure 2c), primarily owing to an additional vibrational relaxation channel offered to $\nu(^{13}C)$ by resonant energy transfer to the aforementioned combination band.

Excited state dynamics without IR excitation

To monitor each of the two charge separation pathways in **1*** independently, time-resolved infrared spectroscopy (TRIR, UV_{pump}-IR_{probe} pulse sequence) is used. TRIR is particularly suited to interrogate charge transfer excited states in Pt-acetylides[27,28] as the C≡C stretch frequency in the ~2000 cm^{-1} region is highly sensitive to its structural and electronic environment, providing an excellent probe of electron transfer dynamics. Figure 3b shows TRIR spectra for **1*** in CH_2Cl_2 in the region of ν(C≡C) at representative time delays following 400 nm, ~50 fs excitation into the MLCT transition (see Supplementary Information for details of the analysis including fingerprint region data, 1500-1800 cm^{-1}). At a 2 ps pump-probe delay, MLCT features dominate with broadened bands at 2016 cm^{-1} and 2104 cm^{-1}. At 50 ps, two structured bands at 2023 cm^{-1} and 2108 cm^{-1}, corresponding to ν(CC) in ^{13}CSS and ^{12}CSS, respectively, are observed. 2DIR experiments performed on the CSS excited states (transient 2DIR, Supplementary Fig. 10-11) provide evidence that $\nu(^{12}C)$ and $\nu(^{13}C)$ are still vibrationally decoupled despite significant changes in electronic distribution compared to the ground state.

As is typical with charge transfer transition metal complexes in solution, many processes occur within the first few picoseconds following excitation into the singlet MLCT band, including vibrational relaxation from the Franck-Condon active modes to a bath of intramolecular low-frequency modes, internal conversion amongst several close-lying metal-to-ligand charge transfer states, solvent reorganization, and intersystem crossing to the triplet manifold.[29] Following this cascade of events, most excess vibrational energy from the excitation pulse is still contained in the solute when the ^{3}MLCT state is populated. It is well-known that the vibrational quantum state on a reactant surface can severely influence the ensuing excited state dynamics.[30–34] Indeed, we find in our ultrafast experiments that the CSSs are formed on two distinct timescales representing ET from a hot ^{3}MLCT (^{3}MLCT*) ($\tau_{hot} = 3.6$ ps) and a relaxed ^{3}MLCT ($\tau_{cool} = 14.7$ ps). Note however that we do not find any evidence of $\nu(C{\equiv}C)_{v>0}$ population in the TRIR data beyond the instrument-limited time resolution of

ca. 250 fs (e.g. compare Figure 3, panels b and c). This observation is not surprising since IVR in these organometallic complexes is typically extremely rapid in the Franck -Condon region.[4,35] and therefore the excess vibrational energy populates lower-frequency intramolecular modes that are nonetheless not readily accessible at room temperature (see Supplementary Fig. 7 for the results of a temperature-dependence study of charge separation dynamics).

Control of ET pathways using targeted vibrational excitation

In order to exert control over ET pathways, we introduce a narrow-band (FWHM 12 cm^{-1}) IR_{pump} pulse 2 ps after 400 nm excitation, when ^{3}MLCT* is populated in the vast majority of UV-excited molecules. The IR_{pump} pulse is chopped at half the UV_{pump} repetition rate, allowing recording a double-difference signal TRIR{IR_{pump}(ON-OFF)}, reliably extracting small signals with negligible systematic error. Figure 3c displays this quantity when exciting either $\nu(^{13}C)$ (left panel) and $\nu(^{12}C)$ (right panel) in ^{3}MLCT*, i.e. at 2016 cm^{-1} and 2104 cm^{-1}, respectively. The immediate effect of the IR_{pump} is to excite $\nu(C{\equiv}C)_{v=0}$ into v = 1, resulting in the bleach-transient peak pair which forms the dominant signal in both panels.[26] The vibrational lifetimes of $\nu(^{13}C)$ and $\nu(^{12}C)$ in ^{3}MLCT extracted from the decay of this transient response (Supplementary Fig. 11) are $\tau(^{13}C)$ = 1.0 ± 0.4 ps, $\tau(^{12}C)$ = 3.6 ± 0.4 ps, somewhat shorter than in the ground state.

The key observation from these experiments is the presence of the off-diagonal signal: a response appearing from the mode that isn't pumped. This feature is most evident when pumping $\nu(^{13}C)$: a transient at 2108 cm^{-1} grows in 3-5 ps after IR excitation. The transient is at the position of the $\nu(^{12}C)$ spectral signature in ^{12}CSS. The off-diagonal signal is not due to vibrational coupling or energy transfer between $\nu(^{13}C)$ and $\nu(^{12}C)$ – such coupling would give rise to a (negative) bleach of the $\nu(^{12}C)_{v=0}$ absorption and to a (positive) transient redshifted from the bleach, resembling the negative-positive peak pair of the diagonal signal. Instead, the exclusive presence of a positive transient signal at the frequency characteristic for $\nu(^{12}C)$ in ^{12}CSS suggests that more ^{12}CSS is formed compared to the case without vibrational excitation. The opposite is true when pumping $\nu(^{12}C)$ in ^{3}MLCT: more ^{13}CSS is formed when the IR pump is present, evidenced by the positive transient at 2023 cm^{-1}. As the two CSSs equilibrate, the off-diagonal transient signal disappears, since no permanent change in the 100% (^{12}CSS + ^{13}CSS) yield is induced by IR excitation. These results are quantitatively reproducible across a range of IR pump powers and sample concentrations, with standard deviations across four datasets quoted below.

To extract the different processes that contribute to the response of **1*** to vibrational perturbation, we use numerical modelling to reproduce the kinetic evolution observed in Figure 3c. This is necessary because the frequencies of $\nu(C{\equiv}C)$ in ^{3}MLCT and CSS are too similar – the diagonal vibrational signal precludes a straightforward analysis of the effect of vibrational excitation on the electronic dynamics of the IR-pumped pathway. The TRIR data in the fingerprint region (1500-1800 cm^{-1}) are free of signals related to vibrational excitation immediately after the IR pump in the ~2000 cm^{-1} region, providing a handle on the electronic response to vibrational perturbation. Furthermore, the signals in the fingerprint region report on changes in electron density on the acceptor ν(CO) at 1730 cm^{-1} and on the aromatic entities, but not of the bridge, making them unselective over which of the two CSSs is affected. From these data (Supplementary Fig. 6, 8, and Supplementary Information section 6) we find that injecting additional vibrational energy accelerates the decay of ^{3}MLCT* into CSSs by 14 ± 2%; this acceleration is to be expected since we already know from pump-probe data that ^{3}MLCT decays to the CSSs faster in the presence of excess vibrational energy (c.f. lifetimes of ^{3}MLCT* compared to ^{3}MLCT), similarly to a range of other Pt-acetylide charge transfer systems in solution.[35,36]

Taking into account this rate acceleration, we then proceed to fit the off-diagonal kinetic response from Figure 3c. The two free parameters to optimize are the equilibration rate between the two CSSs and the relative rate difference, if any, between the two charge-separation pathways. The former is globally fitted across both IR pump frequencies. All other parameters are kept fixed at the measured values, including an empirical factor that properly relates the arbitrary population units of the numerical simulation to the observed signal strength for IR pumped molecules (Supplementary Information, Section 6). We begin with the assumption that in the absence of vibrational perturbation, the two CSSs are populated at the same rate from ^{3}MLCT*, $(18.1\ ps)^{-1}$, justified by the virtually identical kinetic evolution of the excited states in the unlabelled, monolabelled and fully ^{13}C- labelled model complexes obtained in ultrafast transient absorption measurements (Supplementary Fig. 3).

The results of the kinetic modelling are shown in Figure 4. The equilibration rate is found to be $(13.3 \pm 0.9\ ps)^{-1}$. When pumping $\nu(^{13}C)$, the ^{12}CSS formation rate increases from $(18.1\ ps)^{-1}$ to $(10.7\ ps)^{-1}$, a $69 \pm 10\%$ acceleration, whilst the ^{13}CSS formation rate is decreased by $41 \pm 10\%$, to $(30.5\ ps)^{-1}$. When pumping $\nu(^{12}C)$, the opposite effect, albeit less pronounced, is observed: the ^{13}CSS pathway is accelerated to $(14.0\ ps)^{-1}$, a $29 \pm 8\%$ rate increase, while the rate of formation of ^{12}CSS changes to $(18.3\ ps)^{-1}$, a $1 \pm 8\ \%$ (i.e. negligible) rate decrease.

It is important to distinguish the two effects caused by vibrational excitation. One effect is the non-discriminative overall acceleration of ET that could be similarly achieved using shorter-wavelengths electronic excitation, as observed in other Pt-acetylide complexes.[36] The second outcome is a spatial pathway-specific perturbation that has never been achieved previously. This latter effect causes an efficient and selective deceleration of the pumped pathway*:* when $\nu(^{13}C)$ is pumped, formation of the ^{12}CSS becomes the preferred pathway and vice versa.

The results indicate that the IR-control effect is more than twice as efficient when $\nu(^{13}C)$ is pumped than when $\nu(^{12}C)$ is pumped. We also know that IVR from $\nu(^{13}C)_{v=1}$ occurs at a faster rate than charge separation, in large part due to a resonant combination mode that acts as a vibrational energy sink, while IVR from $\nu(^{12}C)_{v=1}$ occurs concurrently with charge separation (Figure 2 and Supplementary Fig. 11). Taken together, these observations suggest that the charge separation reaction co-ordinate whose perturbation is responsible for the IR-control effect is unlikely to be ν(C≡C); instead, a set of local lower-frequency modes that are strongly coupled to ν(C≡C) and that are thus efficiently populated from the latter are likely candidates. These lower-frequency modes are inherently more delocalized than the isolated high frequency stretching mode, and involve collective motion along several bond trajectories. Nevertheless, the lack of vibrational cross-peaks in our 2DIR data show that the population density for these modes remains primarily localized on the excited 'arm' of the molecule. In this way, the high frequency stretch acts as an energy funnel:[37] it facilitates the deposition of a significant amount of vibrational energy into low and mid-frequency modes in a spatially selective way without necessarily being directly involved in the IR-control effect. The absence of a resonant combination mode at the $\nu(^{12}C)$ frequency results in a weaker effect when $\nu(^{12}C)$ is IR-excited because much of the energy doesn't reach these key reaction coordinates during charge separation.

As aforementioned, a crucial condition for the pathway-selective effect to work is that the two IR-excitable vibrations are de-coupled from each other to avoid vibrational excitation becoming rapidly non-selective. Isotopic substitution is one way to achieve this condition. Another important component in our system is the metal centre which acts as a vibrational energy transfer bottleneck that contributes to the localization of injected quanta of energy on either arm of the molecule.[38–42] Furthermore, the presence of the metal offering a two-step charge-separation process starting from a

metal-to-acceptor charge transfer followed by reductive quenching from the donor is a particularly effective design strategy to achieve IR-control:[15,16,35,36] it allows the rapid population of a far-from-equilibrium gateway state where an IR pump can be introduced, and in this way perturb an otherwise symmetrical system in a spatially selective manner at a crucial crossroad where small structural and energetic fluctuations dictate the chosen electronic pathway.[43] Complementary to such excited state evolution is the ability to delay the control pulse with respect to actinic excitation, thus influencing reactivity at the decisive moments of light-induced molecular function[44–47] and circumventing the myriad of processes occurring immediately after electronic excitation, which would rapidly scramble the selectivity of mode-specific excitation.

Conclusion

This study demonstrates, for the first time, the power of mode-specific vibrational perturbation to actively direct electronic transitions in the condensed phase along spatially distinct but electronically identical parallel pathways. To achieve such vibrational control, molecular design is the key: our strategy is to isotopically label one of the two bridges connecting two identical electron donor sites to one acceptor site in a charge-transfer assembly. Such labelling enables both selective vibrational excitation and independent monitoring of the two electron transfer pathways. We find that in this two-way molecular system, excitation of bridging modes during UV-induced charge separation can be used to control the direction of electron transfer: the pathway that is vibrationally excited is dramatically slowed down compared to its counter-part, thus enabling us to choose which path is preferentially taken at the "molecular road-fork". This work contributes to a growing consensus that vibronic coupling, which plays a significant role in nature, may be passively or actively exploited in rational designs of molecular devices that rely on charge and energy transport.

Methods

The synthesis and characterization of **1*** and ^{13}**1** are reported in detail in ref[24].

All ultrafast experiments were performed at the ULTRA facility[48] at the Rutherford Appleton Laboratories, UK. Two synchronized 10 kHz titanium sapphire oscillator/regenerative amplifiers (Thales) pump a range of optical parametric amplifiers (TOPAS). For IR experiments, the instrument uses optical choppers modulating the repetition rate of the UV pump at 5 kHz and IR pump at 2.5 kHz while the probe pulse is at 10 kHz, facilitating the simultaneous collection of background, $\{UV_{pump}\ IR_{probe}\}$ (TRIR); $\{IR_{pump}\ IR_{probe}\}$; and $\{UV_{pump}\ IR_{pump}\ IR_{probe}\}$ spectra. The UV pump pulse (400 nm) was the second harmonic of an 800 nm, 50 fs, 300 cm^{-1} pulsewidth titanium sapphire laser; the IR pump pulsewidth was 1.5 ps, ~12 cm^{-1}; the IR probe pulsewidth was ca. 100 fs, ~350-400 cm^{-1}, depending on the detection region. The spectral resolution was 2 cm^{-1} per pixel. For the data shown in the text, beam energies were approximately 0.1 μJ/pulse, 0.5 μJ/pulse and 0.8 μJ/pulse with spot sizes of approximately 80, 120 and 160 μm for IR probe, IR pump, and UV pump respectively. All experiments were performed well within the linear excitation regime (see supplementary information, section S5). UV and IR pumps were at parallel polarization to each other, while the probe beam was set at magic angle with respect to these pumps. Samples were flown and rastered in Harrick cells with path lengths of 500-640 μm. The results are reproducible across a broad range of IR pump energies and sample concentrations; the final errors are standard deviations across four different datasets normalized to the number of $UV+IR_{pump}$ photons absorbed in the probed volume. UV-Vis absorption and FTIR spectra were taken before and after every experiment to ensure that no photo-decomposition

affected the results. Optical densities at the excitation wavelength (400 nm, $\varepsilon = 5046\ M^{-1}cm^{-1}$) were kept at ≤0.8.

The data in the text and supplementary information are presented as-obtained with no post-processing apart from baseline subtraction. All data for Figures 2-4 and for the figures in the supplementary information are available from the authors.

References

1. Fleming, G. R. & Ratner, M. A. Grand challenges in basic energy sciences. *Phys. Today* **61,** 28–33 (2008).

2. Barbara, P. F., Meyer, T. J. & Ratner, M. A. Contemporary Issues in Electron Transfer Research. *J. Phys. Chem.* **100,** 13148–13168 (1996).

3. Schrauben, J. N., Dillman, K. L., Beck, W. F. & McCusker, J. K. Vibrational coherence in the excited state dynamics of Cr(acac)3: probing the reaction coordinate for ultrafast intersystem crossing. *Chem. Sci.* **1,** 405–410 (2010).

4. Auböck, G. & Chergui, M. Sub-50-fs photoinduced spin crossover in [Fe(bpy)3]2+. *Nat. Chem.* **7,** 629–633 (2015).

5. Johnson, P. J. M. *et al.* Local Vibrational Coherences Drive the Primary Photochemistry of Vision. *Nat. Chem.* **7,** 980–986 (2015).

6. Romero, E. *et al.* Quantum coherence in photosynthesis for efficient solar-energy conversion. *Nat. Phys.* **10,** 676–682 (2014).

7. Fuller, F. D. *et al.* Vibronic coherence in oxygenic photosynthesis. *Nat. Chem.* **6,** 1–6 (2014).

8. Oliver, T. A. A. & Fleming, G. R. Following Coupled Electronic-Nuclear Motion through Conical Intersections in the Ultrafast Relaxation of β-Apo-8′-carotenal. *J. Phys. Chem. B* **119,** 11428–11441 (2015).

9. Tiwari, V., Peters, W. K. & Jonas, D. M. Electronic resonance with anticorrelated pigment vibrations drives photosynthetic energy transfer outside the adiabatic framework. *Proc. Natl. Acad. Sci. U. S. A.* **110,** 1203–8 (2013).

10. Christensson, N., Kauffmann, H. F., Pullerits, T. & Mančal, T. Origin of long-lived coherences in light-harvesting complexes. *J. Phys. Chem. B* **116,** 7449–7454 (2012).

11. Chin, A. W. *et al.* The role of non-equilibrium vibrational structures in electronic coherence and recoherence in pigment–protein complexes. *Nat. Phys.* **9,** 113–118 (2013).

12. Lin, Z. *et al.* Modulating unimolecular charge transfer by exciting bridge vibrations. *J. Am. Chem. Soc.* **131,** 18060–18062 (2009).

13. Yue, Y. *et al.* Electron transfer rate modulation in a compact Re(i) donor-acceptor complex. *Dalton Trans.* **44,** 8609–8616 (2015).

14. Bakulin, A. a. *et al.* Mode-selective vibrational modulation of charge transport in organic electronic devices. *Nat. Commun.* **6,** 7880 (2015).

15. Delor, M. *et al.* Toward control of electron transfer in donor-acceptor molecules by bond-specific infrared excitation. *Science* **346,** 1492–1495 (2014).

16. Delor, M. *et al.* On the mechanism of vibrational control of light-induced charge transfer in donor–bridge–acceptor assemblies. *Nat. Chem.* **7,** 689–695 (2015).

17. Skourtis, S. S., Waldeck, D. H. & Beratan, D. N. Inelastic Electron Tunneling Erases Coupling-Pathway Interferences. *J. Phys. Chem. B* **108,** 15511–15518 (2004).

18. Xiao, D., Skourtis, S. S., Rubtsov, I. V & Beratan, D. N. Turning charge transfer on and off in a molecular interferometer with vibronic pathways. *Nano Lett.* **9,** 1818–1823 (2009).

19. Carias, H., Beratan, D. N. & Skourtis, S. S. Floquet analysis for vibronically modulated electron tunneling. *J. Phys. Chem. B* **115,** 5510–5518 (2011).

20. Antoniou, P., Ma, Z., Zhang, P., Beratan, D. N. & Skourtis, S. S. Vibrational Control of Electron-Transfer Reactions: a Feasibility Study for the Fast Coherent Transfer Regime. *Phys. Chem. Chem. Phys.* **17,** 30854–30866 (2015).

21. McGarrah, J. E. & Eisenberg, R. Dyads for photoinduced charge separation based on platinum diimine bis(acetylide) chromophores: synthesis, luminescence and transient absorption studies. *Inorg. Chem.* **42,** 4355–65 (2003).

22. Sazanovich, I. V. *et al.* Ultrafast photoinduced charge transport in Pt(II) donor–acceptor assembly bearing naphthalimide electron acceptor and phenothiazine electron donor. *Phys. Chem. Chem. Phys.* **16,** 25775–25788 (2014).

23. McGarrah, J. E., Hupp, J. T. & Smirnov, S. N. Electron transfer in platinum(II) diimine-centered triads: mechanistic insights from photoinduced transient displacement current measurements. *J. Phys. Chem. A* **113,** 6430–6 (2009).

24. Archer, S. A., Keane, T., Delor, M., Meijer, A. J. H. M. & Weinstein, J. A. 13 C or Not 13 C: Selective Synthesis of Asymmetric Carbon-13-Labeled Platinum(II) cis -Acetylides. *Inorg. Chem.* **55,** 8251–8253 (2016).

25. Lipkin, J. S., Song, R., Fenlon, E. E. & Brewer, S. H. Modulating Accidental Fermi Resonance: What a Difference a Neutron Makes. *J. Phys. Chem. Lett.* **2,** 1672–1676 (2011).

26. Hamm, P. & Zanni, M. *Concepts and Methods of 2D Infrared Spectroscopy*. (Cambridge University Press, 2011).

27. Glik, E. A. *et al.* Ultrafast Excited State Dynamics of Pt(II) Chromophores Bearing Multiple Infrared Absorbers. *Inorg. Chem.* **47,** 6974–6983 (2008).

28. Archer, S. & Weinstein, J. A. Charge-separated excited states in platinum(II) chromophores: Photophysics, formation, stabilization and utilization in solar energy conversion. *Coord. Chem. Rev.* **256,** 2530–2561 (2012).

29. McCusker, J. K. Femtosecond absorption spectroscopy of transition metal charge-transfer complexes. *Acc. Chem. Res.* **36,** 876–87 (2003).

30. Spears, K. G., Wen, X. & Zhang, R. Electron Transfer Rates from Vibrational Quantum States. *J. Phys. Chem.* **100,** 10206–10209 (1996).

31. Crim, F. F. Bond-Selected Chemistry : Vibrational State Control of Photodissociation and Bimolecular Reaction. *J. Phys. Chem.* **100,** 12725–12734 (1996).

32. Crim, F. F. Chemical dynamics of vibrationally excited molecules: Controlling reactions in gases and on surfaces. *Proc. Natl. Acad. Sci. U. S. A.* **105,** 12654–12661 (2008).

33. Roberts, G. M. *et al.* Exploring quantum phenomena and vibrational control in σ* mediated photochemistry. *Chem. Sci.* **4,** 993–1001 (2013).

34. Nazarov, A. E., Barykov, V. Y. & Ivanov, A. I. Effect of Excitation Pulse Carrier Frequency

on Ultrafast Photoinduced Charge Transfer Kinetics: Effect of Intramolecular High Frequency Vibrational Mode Excitation. *J. Phys. Chem. C* **119,** 2989–2995 (2015).

35. Delor, M., Sazanovich, I. V., Towrie, M. & Weinstein, J. A. Probing and Exploiting the Interplay between Nuclear and Electronic Motion in Charge Transfer Processes. *Acc. Chem. Res.* **48,** 1131–1139 (2015).

36. Scattergood, P. A. *et al.* Electron Transfer Dynamics and Excited state Branching in a Charge-Transfer Platinum(II) Donor-Bridge-Acceptor Assembly. *Dalt. Trans.* **43,** 17677–17693 (2014).

37. Antoniou, P., Ma, Z., Zhang, P., Beratan, D. N. & Skourtis, S. S. Vibrational control of electron-transfer reactions: a feasibility study for the fast coherent transfer regime. *Phys. Chem. Chem. Phys.* **17,** 30854–30866 (2015).

38. Kasyanenko, V. M., Lin, Z., Rubtsov, G. I., Donahue, J. P. & Rubtsov, I. V. Energy transport via coordination bonds. *J. Chem. Phys.* **131,** 154508 (2009).

39. Rubtsov, I. V. Relaxation-Assisted Two-Dimensional Infrared (RA 2DIR) Method: Accessing Distances over 10 Å and Measuring Bond Connectivity Patterns. *Acc. Chem. Res.* **42,** 1385–1394 (2009).

40. Park, K.-H. *et al.* Infrared Probes Based on Nitrile-Derivatized Prolines: Thermal Insulation Effect and Enhanced Dynamic Range. *J. Phys. Chem. Lett.* **4,** 2105–2110 (2013).

41. Delor, M. *et al.* Dynamics of ground and excited state vibrational relaxation and energy transfer in transition metal carbonyls. *J. Phys. Chem. B* **118,** 11781–91 (2014).

42. Fedoseeva, M. *et al.* Vibrational energy transfer dynamics in ruthenium polypyridine transition metal complexes. *Phys. Chem. Chem. Phys.* **17,** 1688–1696 (2015).

43. Dereka, B., Rosspeintner, A., Li, Z., Liska, R. & Vauthey, E. Direct Visualization of Excited-State Symmetry Breaking Using Ultrafast Time-Resolved Infrared Spectroscopy. *J. Am. Chem. Soc.* **138,** 4643–4649 (2016).

44. Dorfman, K. E., Zhang, Y. & Mukamel, S. Coherent control of long-range photoinduced electron transfer by stimulated X-ray Raman processes. *Proc. Natl. Acad. Sci.* **113,** 10001–10006 (2016).

45. Vogt, G., Nuernberger, P., Brixner, T. & Gerber, G. Femtosecond Pump – Shaped-Dump Quantum Control of Retinal Isomerization in Bacteriorhodopsin. *J. Chem. Phys. Lett.* **433,** 211–215 (2006).

46. Dietzek, B., Bruggemann, B., Pascher, T. & Yartsev, A. Pump-Shaped Dump Optimal Control Reveals the Nuclear Reaction Pathway of Isomerization of a Photoexcited Cyanine Dye. *J. Am. Chem. Soc.* **129,** 13014–13021 (2007).

47. Debreczeny, M. P., Svec, W. A., Marsh, E. M. & Wasielewski, M. R. Femtosecond Optical Control of Charge Shift within Electron Donor - Acceptor Arrays : An Approach to Molecular Switches. *J. Am. Chem. Soc.* **118,** 8174–8175 (1996).

48. Greetham, G. *et al.* ULTRA: A unique instrument for time-resolved spectroscopy. *Appl. Spectrosc.* **64,** 1311–1319 (2010).

Acknowledgements

Financial support of the EPSRC, the E-Futures Doctoral training Centre, the University of Sheffield, and the STFC, including access to beam time, is gratefully acknowledged. We thank A. W. Parker for

inspiring discussions, and E. Greenough, G. Farrow, A. Auty, and A. Sadler for help with variable temperature measurements.

Author contributions

M.D. and J.A.W. conceived the hypothesis, M. D., I. V. S. and J.A.W. designed the experiments. M.D., S.A.A. and I.V.S. conducted the experiments on a set-up built and operated by M.T., G.M.G. and I.V.S. M.D. analysed the experimental data. S.A.A. synthesized the molecules. T.K. and A.J.H.M.M. performed supporting DFT calculations. M.D. and J.A.W. wrote the paper, with input from all authors.

Additional information

Supplementary information contains descriptions of experimental methods (S1), ultrafast transient absorption (S2), computational investigations (S3), additional time-resolved IR and IR-control data (S4), additional 2-dimensional infrared spectroscopy data (S5) and details on the numerical modelling (S6).

Correspondence should be addressed to M.D. (milan.delor@berkeley.edu) and J.A.W (julia.weinstein@sheffield.ac.uk).

Competing financial interests

The authors declare no competing financial interests.

Figure Captions

Figure 1. Summary of the multipulse IR-control experiments. (a) Hypothesis: directing electron transfer along a preselected pathway in a D─B─A─B─D system. (b) Asymmetrically isotopically labelled D─B─A─^{13}B─D molecular "fork" **1***. (c) Pulse sequence used for IR-control experiments, UV_{pump}-IR_{pump}-IR_{probe}. The IR pump frequency is tuned to the $^{12}C{\equiv}^{12}C$ or $^{13}C{\equiv}^{13}C$ acetylide stretching frequency at the "gateway" excited state, i.e. in the hot triplet metal-to-ligand charge transfer state (^{3}MLCT*) as it is about to decay to a charge-separated state with the hole located either on donor 1 (^{12}CSS) or donor 2 (^{13}CSS). (d) Energy level diagram of the excited state pathways of **1*** in CH_2Cl_2 following UV_{pump} (400 nm, 50-fs) excitation.

Figure 2. Ground state infrared absorption properties of 1* in CD_2Cl_2. (a) FTIR spectrum; (b) Ground state 2-dimensional infrared (2DIR) spectrum at 3 ps IR_{pump}-IR_{probe} delay. The lack of off-diagonal features shows that ν(^{13}C) and ν(^{12}C) are successfully de-coupled using isotopic substitution; (c) Corresponding IR_{pump}-IR_{probe} kinetic traces and fits at the positions denoted by 'x' in (b), collected by fixing the IR pump frequency and recording probe slices at several time delays. Solid lines are Gaussian IRF-convolved single-exponential fits to the data. The vibrational relaxation time of ν(^{13}C) is much shorter than that of ν(^{12}C) due to an additional relaxation pathway offered by the resonant combination mode.

Figure 3. Summary of excited state dynamics with and without vibrational perturbation in CH_2Cl_2, with the left panel showing results for ν(^{13}C) excitation and the right panel for ν(^{12}C) excitation (2016 cm^{-1} and 2104 cm^{-1}, respectively). (a) FTIR of **1***. (b) TRIR spectra at 2 and 50 ps time delay following 400 nm excitation, displaying the spectral profiles of ν(^{12}C) and ν(^{13}C) in ^{3}MLCT* and CSS, respectively. The apparent difference in shape of the ^{12}CSS vs. ^{13}CSS TRIR signals is due to a larger bleach/transient overlap for the latter. (c) IR-control experiments: the IR_{pump} is introduced 2 ps after the UV_{pump}, and the spectra shown are recorded with the IR_{probe} at 1 ps (black), 3 ps (green) and 50 ps (blue) after the IR_{pump} (kinetic traces are shown in Fig. 4). The bleach-transient peak pairs are signatures of de-population of the v = 0 and population of the v = 1 state of the excited mode. The off-diagonal signals arising at frequencies not excited by the IR_{pump} are due to a change in electronic dynamics, specifically the rate of formation of the ^{12}CSS and ^{13}CSS (see text for details). The presence and sign of the off-diagonal signals suggests that vibrational excitation of one pathway accelerates electron transfer through the opposite pathway. More information is given in Supplementary Figs. 5-11.

Figure 4. Modelling of the kinetic evolution of the off-diagonal response in IR-control experiments. (a, b) Plain circles show the kinetic evolution of the integrated off-diagonal peaks in Figure 3c, while solid lines are the results of the numerical model detailed in the text. The dashed line shows the expected signal should the IR pump accelerate both pathways symmetrically. (c, d) The overall concentration profiles of each modelled state starting from ^{3}MLCT*. The profile of either CSS in the case of no IR excitation is shown with the black dashed line. When ν(^{13}C) is excited, the ^{12}CSS pathway is preferentially accelerated, and vice versa, leading to a transient change in the population of both CSS states. These changes disappear as the two CSSs re-equilibrate with τ_{equil} = 13.3 ± 0.9 ps.

Directing the path of light-induced electron transfer at a molecular fork using vibrational excitation

Milan Delor,[1#] Stuart A. Archer,[1] Theo Keane,[1] Anthony J.H.M. Meijer,[1] Igor V. Sazanovich,[2] Gregory M. Greetham,[2] Michael Towrie,[2] and Julia A. Weinstein[1*]*

Table of content:

Ultrafast vibrational excitation directs light-induced intramolecular electron transfer along a pathway chosen at will

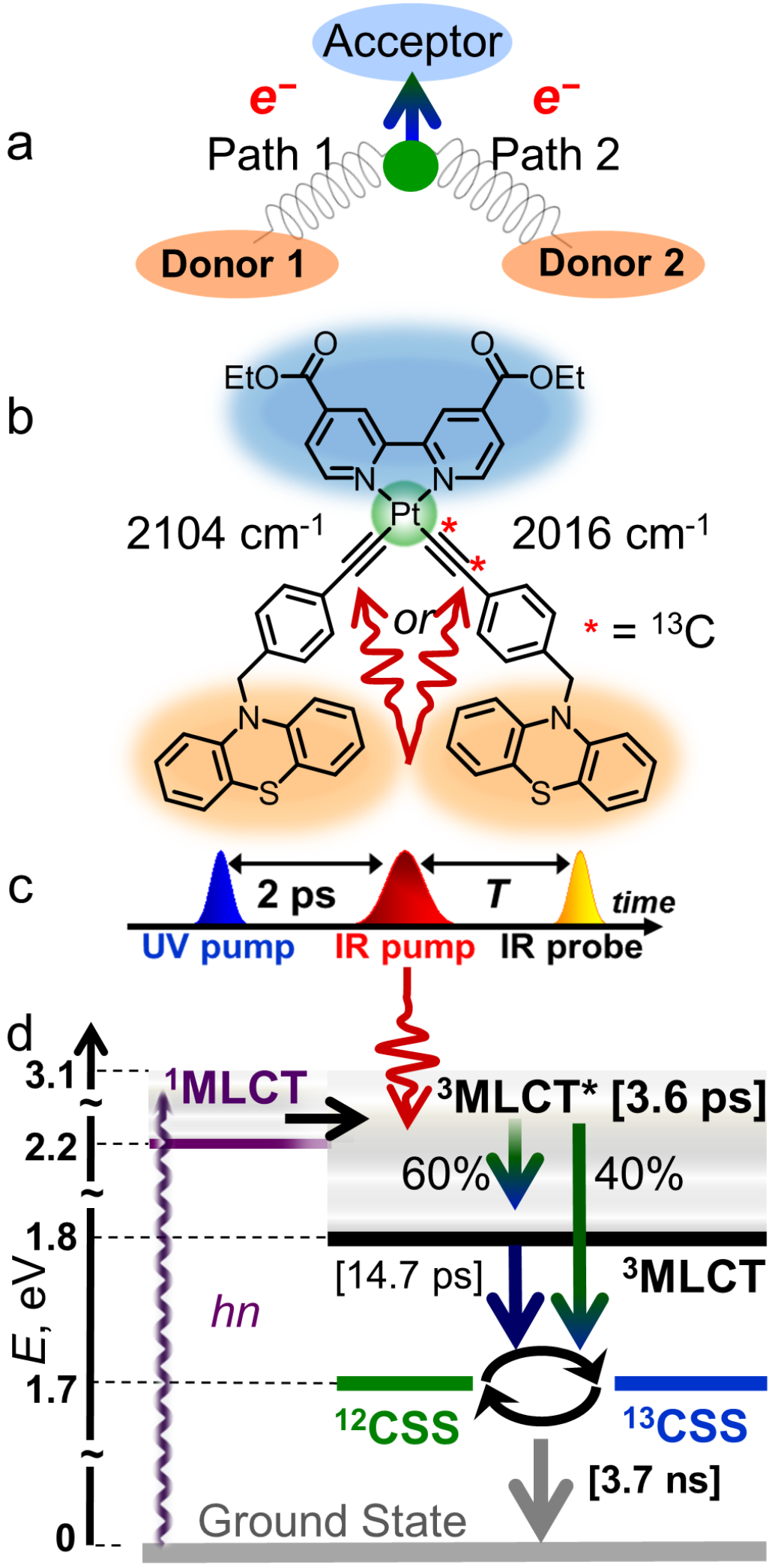
a
Acceptor
e⁻
e⁻
Path 1
Path 2
Donor 1
Donor 2
b
EtO
OEt
O
O
N
N
Pt
2104 cm-1
2016 cm-1
*
*
or
* = 13C
N
S
N
S
c
2 ps
T
time
UV pump
IR pump
IR probe
d
3.1
2.2
1.8
1.7
0
E, eV
1MLCT
3MLCT* [3.6 ps]
60%
40%
[14.7 ps]
3MLCT
hn
12CSS
13CSS
[3.7 ns]
Ground State

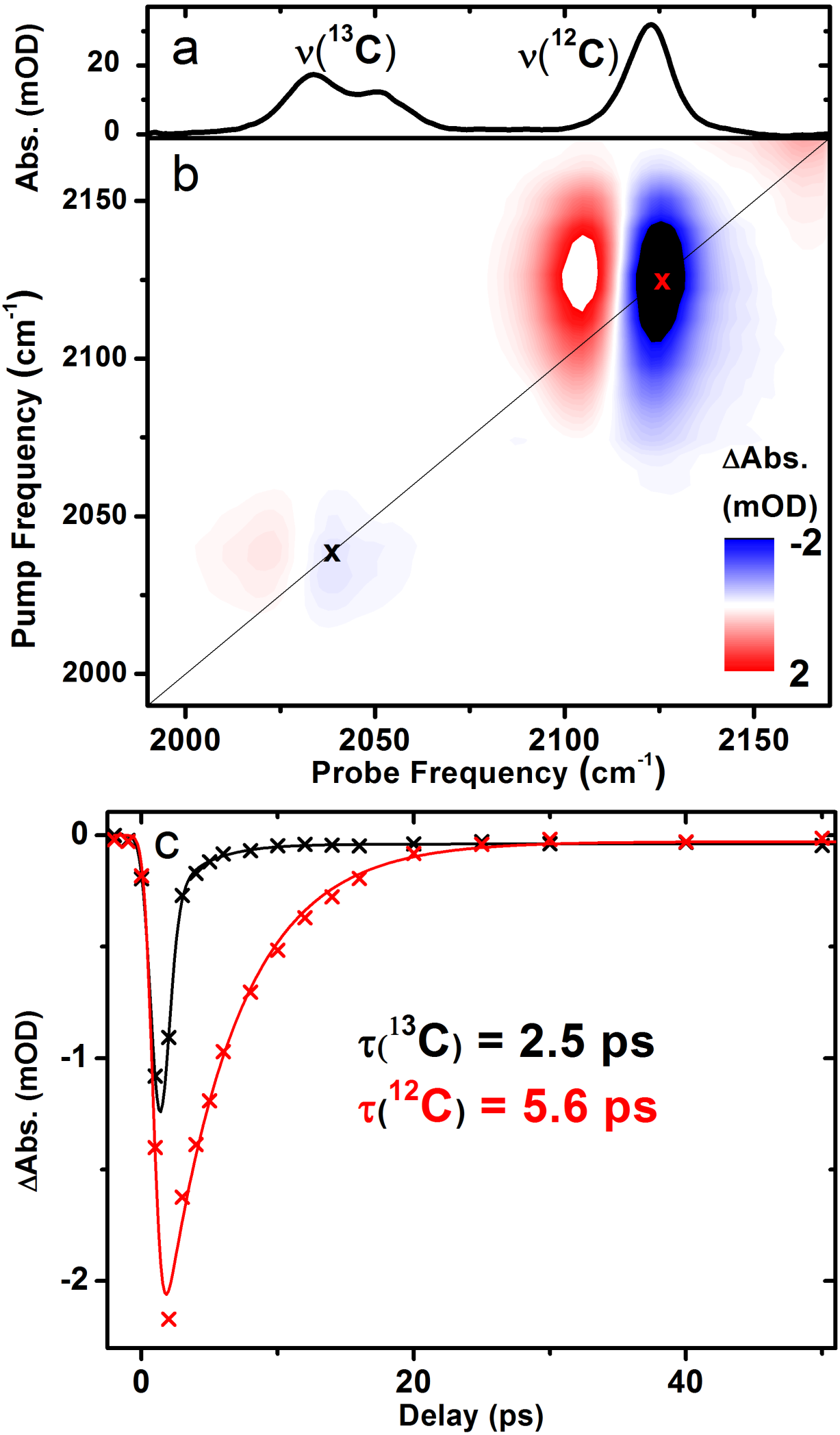
a
ν(13C)
ν(12C)
Abs. (mOD)
20
0
b
Pump Frequency (cm-1)
2150
2100
2050
2000
ΔAbs.
(mOD)
-2
2
Probe Frequency (cm-1)
2000
2050
2100
2150
c
ΔAbs. (mOD)
0
-1
-2
τ(13C) = 2.5 ps
τ(12C) = 5.6 ps
0
20
40
Delay (ps)

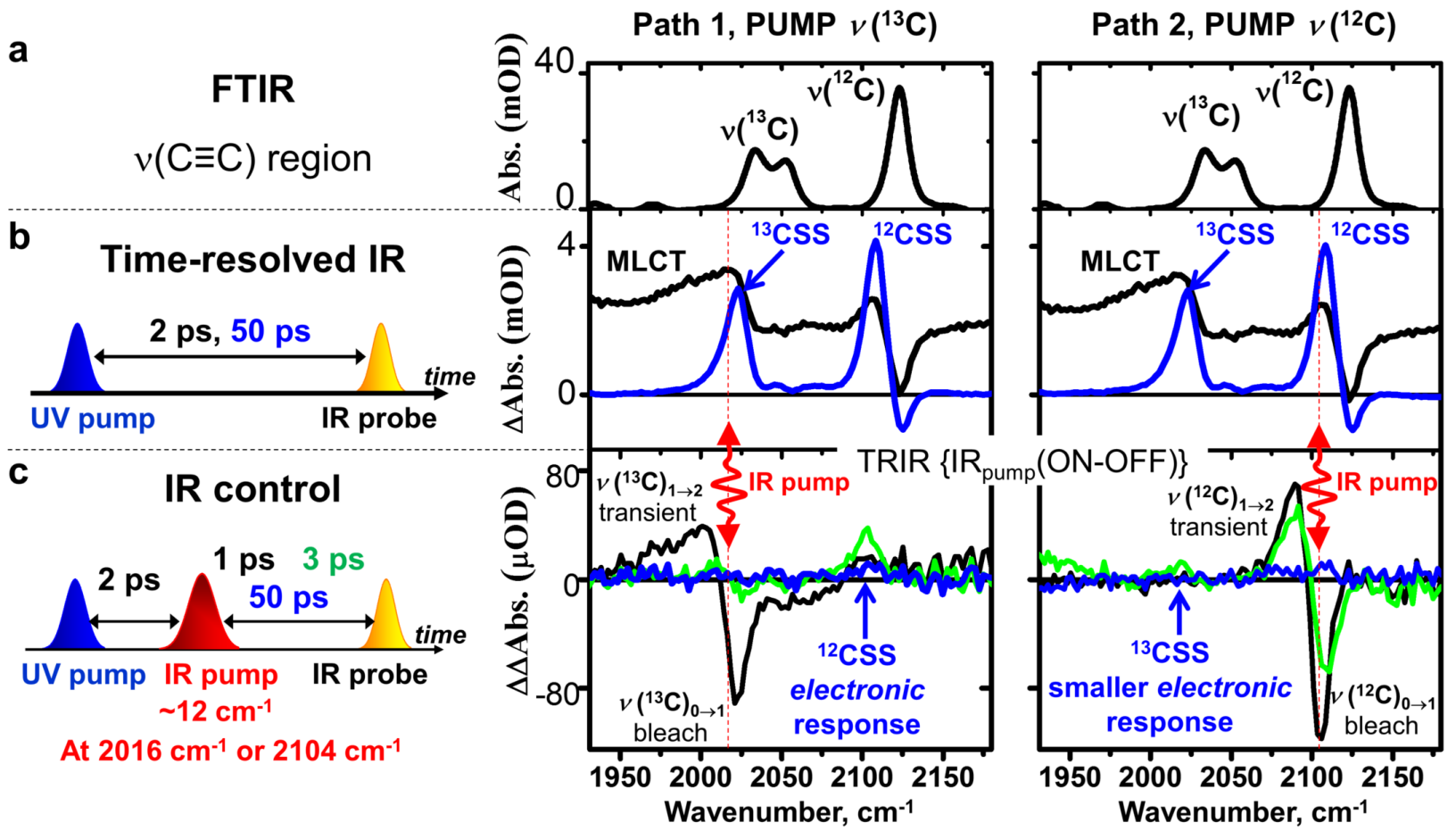
a
FTIR
ν(C≡C) region
b
Time-resolved IR
2 ps, 50 ps
time
UV pump
IR probe
c
IR control
2 ps
1 ps
3 ps
50 ps
time
UV pump
IR pump
IR probe
~12 cm-1
At 2016 cm-1 or 2104 cm-1
Path 1, PUMP ν(13C)
Path 2, PUMP ν(12C)
Abs. (mOD)
ΔAbs. (mOD)
ΔΔAbs. (μOD)
ν(13C)
ν(12C)
MLCT
13CSS
12CSS
TRIR {IRpump(ON-OFF)}
ν(13C)1→2 transient
IR pump
ν(12C)1→2 transient
ν(13C)0→1 bleach
12CSS electronic response
13CSS smaller electronic response
ν(12C)0→1 bleach
Wavenumber, cm-1

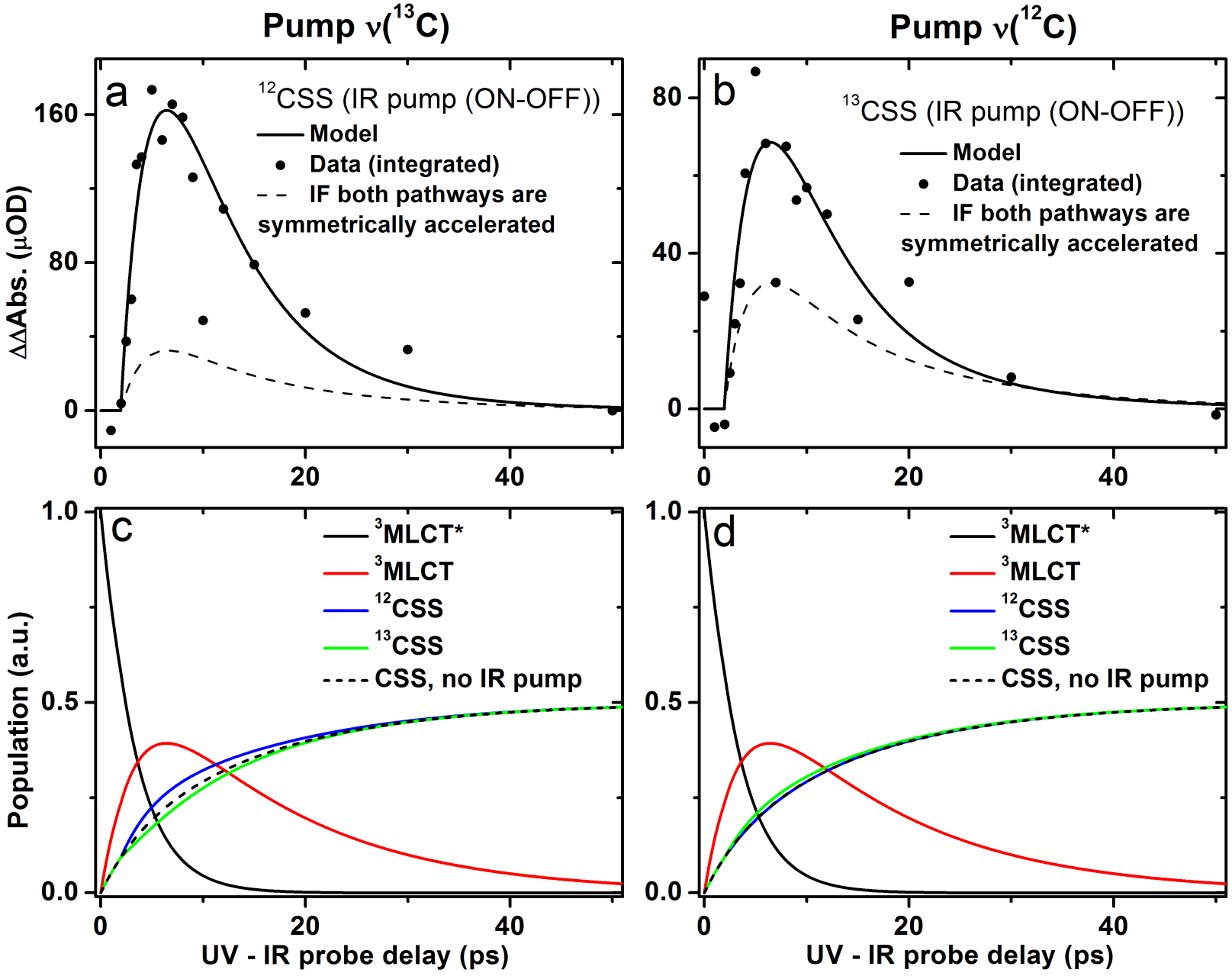
Pump ν(13C)
Pump ν(12C)
a
b
c
d
12CSS (IR pump (ON-OFF))
13CSS (IR pump (ON-OFF))
Model
Data (integrated)
IF both pathways are symmetrically accelerated
ΔΔAbs. (μOD)
Population (a.u.)
UV - IR probe delay (ps)
3MLCT*
3MLCT
12CSS
13CSS
CSS, no IR pump